International Atomic Energy Agency

INDC(NDS)-194
Distr.: L

INDC INTERNATIONAL NUCLEAR DATA COMMITTEE

THE Cf-252 SPONTANEOUS FISSION NEUTRON SPECTRUM IN THE 5-20 MeV ENERGY RANGE

H. Märten, R. Richter, D. Seeliger
Technische Universität Dresden
Deutsche Demokratische Republik

W.D. Fromm
Zentralinstitut für Kernforschung Rossendorf
Deutsche Demokratische Republik

R. Böttger, H. Klein
Physikalisch-Technische Bundesanstalt Braunschweig
Bundesrepublik Deutschland

January 1987

INDC(NDS)-194
Distr.: L

THE Cf-252 SPONTANEOUS FISSION NEUTRON SPECTRUM IN THE 5-20 MeV ENERGY RANGE

H. Märten, R. Richter, D. Seeliger
Technische Universität Dresden
Deutsche Demokratische Republik

W.D. Fromm
Zentralinstitut für Kernforschung Rossendorf
Deutsche Demokratische Republik

R. Böttger, H. Klein
Physikalisch-Technische Bundesanstalt Braunschweig
Bundesrepublik Deutschland

January 1987

Printed by the IAEA in Austria
January 1987

87-03158

The ^{252}Cf(sf) Neutron Spectrum in the 5 - 20 MeV Energy Range

H. Märten, R. Richter and D. Seeliger
Technische Universität Dresden, Sektion Physik
DDR-8027 Dresden, Mommsenstraße 13, GDR
W. D. Fromm
Zentralinstitut für Kernforschung Rossendorf
DDR-8051 Dresden, Postfach 19, GDR
R. Böttger and H. Klein
Physikalisch-Technische Bundesanstalt
D-3300 Braunschweig, Bundesallee 100, FRG

Abstract

The ^{252}Cf neutron spectrum has been measured at high energies with a miniature ionization chamber and two different NE213 neutron detectors. The γ-ray background and the main cosmic background were suppressed by applying an efficient pulse shape $n/(\gamma,\mu)$ discrimination. On the basis of the two-dimensional spectroscopy of neutron time-of-flight and scintillation pulse height, the sliding bias method has been used to minimize experimental uncertainties.

The experimental data corrected for several systematic influences confirm earlier results which show a trend similar to the NBS evaluation. However, the final spectra obtained for both neutron detectors exhibit negative deviations (up to -10 %) from the NBS curve in the 6 - 12 MeV range.

Finally, the experimental results of this work are compared with various statistical-model approaches to the ^{252}Cf(sf) neutron spectrum.

Introduction

Within the framework of the elaboration of the ^{252}Cf neutron spectrum as a well-established standard[1-3], the high energy range is important for fixing a data evaluation at the upper

spectrum tail. Furthermore, this spectrum region can be used as a sensitive test of statistical-model approaches to fission neutron spectra[4].

Previous spectrum data show rather large discrepancies at high neutron energies. The precise measurement of the strongly decreasing neutron spectral yield at high energies requires an efficient suppression of the background (γ-rays, cosmic radiation) and an optimum bias of the neutron detector[4]. The multi-parameter measurement of at least the neutron time-of-flight (TOF) and scintillator pulse height (light output LO) has previously been applied to extend the measurable energy range[5] and to decrease the experimental uncertainties at rather high energies [5,6]. In this work, a new measurement carried out on the basis of a similar, extended method is described. The data deduced are compared with statistical-model approaches reviewed in Ref. 4.

2. Experimental Method

Two neutron detectors with NE213 scintillators were applied under different experimental conditions summarized in Table 1. The main differences concern the scintillator size, the length of the flight path, and the detector position. The experimental arrangement is represented schematically in Fig. 1, which includes a specification of the collimator/shielding set-up of both neutron detectors.

A miniature ionization chamber[6] with a ^{252}Cf source (about 70 000 fissions s^{-1}) was used for fast fission fragment (ff) detection (ΔE chamber). The total fragment detection efficiency deduced from a fragment-neutron correlation measurement[6] was found to be (0.992 ± 0.002).

A scheme of the data processing system is shown in Fig. 2. The two-dimensional (TOF, LO) spectra of both neutron detectors were measured simultaneously using a coupled microcomputer-minicomputer system at ZfK Rossendorf. In addition, several single spectra were recorded to check the stability of the spectrometer during the measurement.

Pulse shape discrimination[7] was applied to efficiently suppress the background. Figures 3 - 6 represent the magnitude of the main background components: γ-rays at rather low LO and cosmic myons at rather high LO. The LO spectrum without particle discrimination exhibits a large myon hump (Fig. 5) which could be reduced to about 0.3 %. The remaining background at high LO is mainly due to cosmic protons and neutrons. For further details of $n/(\gamma;\mu)$ discrimination, see Ref. 5.

Typical neutron spectra are represented in Figures 7 - 9. In particular, Fig. 7 (two-dimensional (TOF, LO) spectrum) illustrates the course of the scintillator response depending on E (cf. Ref. 5b).

Anisotropic losses of ff-events chiefly caused by the roughness of the backing give rise to energy-dependent corrections which also depend on the position of the neutron detector with respect to the backing plane[6] (angle ϑ). These losses were determined by neutron-ff correlation measurements at ϑ = 0°, 60°, 90° which were analyzed for various neutron detection thresholds (Fig. 10). The mean efficiency $\langle\varepsilon\rangle$ = 99.2 %, deduced from the correlated data, is in good agreement with ε_{cf} (60°) as is to be expected[6]. The correlated ΔE spectra (Fig. 11) also demonstrate the exceptional position of this observation angle. While the shape of the 60° spectrum is in very good agreement with the single spectrum (Fig. 11a), the 0° and 90° spectra (Fig. 11b) for the same neutron detector threshold ($E_n > 2$ MeV) differ significantly.

However, the corrections calculated[5b] for this high efficiency are negligible in particular for this high neutron energy region investigated (Fig. 12).

3. Data Analysis

The data analysis procedures considered in this work have also been described in detail elsewhere[5b], hence, only a summary is given here. To obtain minimum experimental uncertainties at high neutron energies, the sliding bias method was applied. The two-dimensional neutron detector efficiency matrix depending on

energy and bias B was calculated using a Monte Carlo code[8] and checked experimentally[5b]. The LO calibration was performed on the basis of γ-ray response functions as well as the measured (TOF, LO) spectra themselves (response function analysis for fixed TOF bins, i.e. selected neutron energy intervals).

The analysis routine involves the determination of the energy spectrum for an eligible B set, i.e. N(E:B). The independence of the spectral yield N(E:B) on B is a sensitive test of LO calibration. The accepted value N(E) is deduced by averaging N(E:B) in the range of minimum total uncertainty. The B range considered extends from 2 to 9 MeV proton energy equivalent for both neutron detectors (i.e. about 0.5 - 5.0 MeV electron energy equivalent).

The measured TOF spectra were corrected for time resolution, TOF bin width, fragment detector efficiency (Fig. 12), background due to non-correlated timing signals, and transmission as described in Refs. 5b and 6. The background due to scattered neutrons was found to be negligible for the energy range considered. The time resolution correction at high energy increases with E. It amounts to about -3 % at 20 MeV for both neutron detectors. The resolution function was considered E-dependent (consequence of scintillator thickness, Ref. 5b). The TOF bin width correction, which increases as E increases, amounts to -0.9 % and -2.7 % at 20 MeV for detectors 1 and 2, respectively. The efficiency of the fission fragment detector applied is close to 1. The corresponding correction is therefore small (cf. Fig. 12). It was calculated analytically as described in Ref. 5b, assuming an idealized angular distribution of fragment losses (Gaussian shape) and taking into account theoretical energy and angular distributions of Cf fission neutrons.

The TOF-channel dependent background due to non-correlated timing signals was also calculated analytically. It is lower than 1 % in the energy range considered. The transmission correction (detector walls, air) is weakly E-dependent at high energies.

Finally, the original point data (E points corresponding to TOF scale) were concentrated by averaging the spectrum deviations

from a reference Maxwellian distribution with a 1.42 MeV "temperature" parameter T for the energy bins considered. The data deduced and the experimental uncertainties for detectors 1 and 2 are listed in Tables 2 and 3, respectively. Both spectra are shown in Figures 13 and 14.

The uncertainties stated include the statistical ones as well as several partial systematic uncertainties (neutron detector efficiency, energy scale, bin width, LO calibration, uncertainties of all corrections stated above, cf. Ref. 5b).

4. Results, Discussion

The measurements carried out with two neutron detectors under different experimental conditions have resulted in quite similar energy distributions of ^{252}Cf neutrons. The high-energy data confirm the trend already stated in the NBS evaluation[9], the negative deviation from the reference Maxwellian (T = 1.42 MeV) at energies higher than 6 MeV. As shown in Figures 13 and 14, the measured data of both detectors are somewhat lower than the NBS spectrum in the 6 - 12 MeV range (deviations up to -10 %), whereas good agreement has been found in the energy region above 14 MeV.

Furthermore, the present experiment confirms earlier data on the high-energy range (9 - 20 MeV) carried out at the TU Dresden[5], yielding a "temperature" parameter of 1.374 MeV from a fit to a Maxwellian distribution.

The high-energy tail of the fission neutron spectrum is very sensitive to its theoretical description.

In particular, the complexity of fission and fission neutron emission, as well as the adequate level density description are most important components of a statistical-model approach to fission neutron spectra.

Recent theoretical treatments have been reviewed elsewhere[4]. The experimental data of this work are compared with the Madland-Nix model (MNM)[10], the Generalized Madland-Nix model

(GMNM)[11], the Cascade Evaporation model (CEM)[12], and a Hauser-Feshbach calculation (HFC)[13] in Figures 15 and 16.

It is remarkable that the MNM and the HFC spectra show a deviation from the reference Maxwellian (T = 1.42 MeV) which increases too strongly at high energies.

The course of the deviation function seems to be more realistic in the case of the GMNM and the CEM. Both these approaches include the consideration of mass and energy distribution in fission up to a certain extent. Here, the CEM is the more complex model based on a fragment distribution in mass, kinetic energy, and excitation energy.

It is concluded that the spectrum range considered can be described by a complex statistical-model approach. Remaining differences between experiment and theory (CEM, GMNM) might be explained by varying the input parameters within their uncertainties[1].

Beyond the spectrum range which is relevant for the ^{252}Cf standard (upper limit 20 MeV), experimental data were deduced up to 30 MeV. These results, already discussed elsewhere[14], indicate a neutron excess in the case of the detector 1 measurement as found earlier[5]. On the other hand, the detector 2 spectrum is in quite good agreement with the Maxwellian up to 25 MeV. However, the rather large uncertainties due to the very low emission rate in this energy range and the remaining background do not allow further conclusions to be drawn. It should be mentioned that the contribution of this background could be reduced or excluded in recent investigations[15,16] which both contradict a neutron excess with reference to a Maxwellian (T = 1.42 MeV).

Acknowledgements

The support of the IAEA and the assistance of Dr. Hermsdorf in calculating the neutron detector efficiencies are gratefully acknowledged.

References

1 Proc. IAEA Consultants' Meeting on the U-235 Fast-Neutron Fission Cross-Section, and the Cf-252 Fission Neutron Spectrum, Smolenice, 1983, INDC(NDS)-146/L (1983)

2 Proc. IAEA Advisory Group Meeting on Nuclear Standard Reference Data, Geel, 1984, IAEA-TECDOC-335 (1985)

3 Proc. IAEA Advisory Group Meeting on Neutron Source Properties, Leningrad, 1986, in press

4 H. Märten, D. Seeliger, loc. cit. (2), p. 255

5 H. Märten et al.,
(a) INDC(GDR)-17/L (1982)
(b) INDC(GDR)-28/L (1984)
(c) Proc. Int. Conf. on Nuclear Data for Science and Technology, Antwerp, 1982, ed. by K.H. Böckhoff, D. Reichel Publ. Comp., Eindhoven (1983) 488

6 R. Böttger et al., Proc. Int. Conf. on Nuclear Data for Science and Technology, Antwerp, 1982, ed. by K.H. Böckhoff, D. Reichel Publ. Comp., Eindhoven (1983) 484

7 H.-G. Ortlepp, Proc. X^{th} Int. Symp. on Nuclear Electronics, Dresden, 1980

8 N.R. Stanton, COO-1545-92 (1971) and D. Hermsdorf, ZfK-315 (1977) 192

9 J. Grundl, C. Eisenhauer, NBS-493 (1977)

10 D.G. Madland et al., loc. cit. (2), p. 267

11 H. Märten, D. Seeliger, INDC(GDR)-30/L (1984)

12 H. Märten, D. Seeliger, loc. cit. (2), p. 279 and J. Phys. G 10 (1984) 349

13 B.F. Gerasimenko, V.A. Rubchenya, loc. cit. (2), p. 280

14 R. Böttger et al., Proc. Int. Conf. on Nuclear Data for Basic and Applied Science, Santa Fe, 1985, ed. by P.G. Young et al., Vol. 2, Gordon and Breach Science Publishers, New York (1986) 1471

15 A. Chalupka et al., loc. cit. (3)

16 W. Mannhart, loc. cit. (3), contributed paper

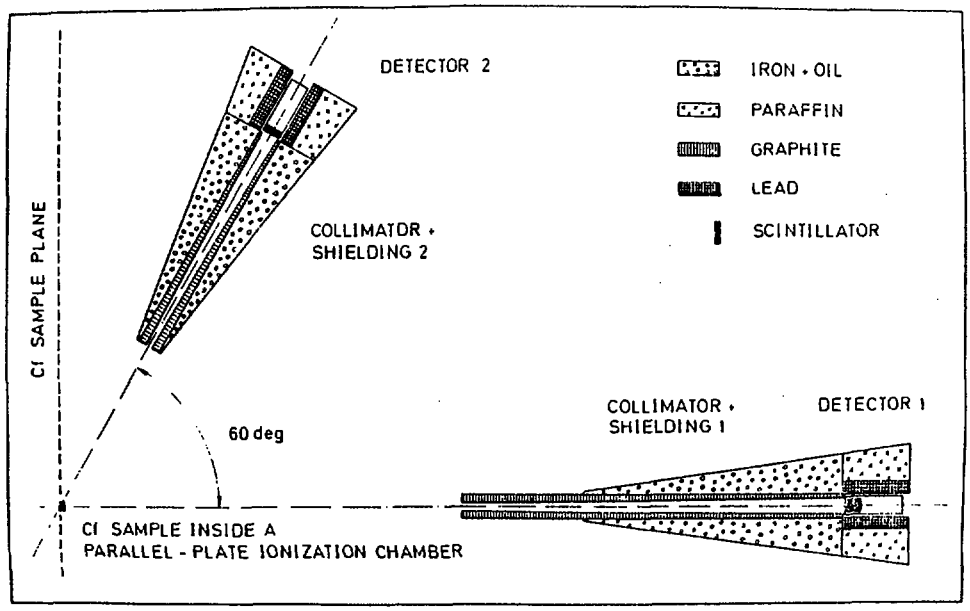

Fig. 1 Scheme of the experimental set-up

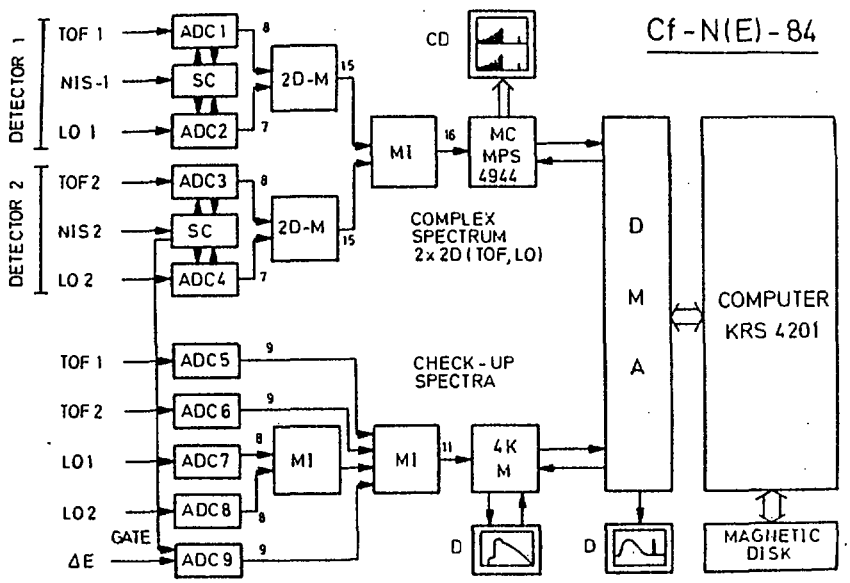

Fig. 2 Schematic representation of data processing (TOF - time-of-flight signal, LO - light output amplitude, Δ E - fission chamber amplitude, NIS - neutron identification signal, ADC - analogue-to-digital converter, SC - slow coincidence, 2D-M - multiplexer interface (two-dimensional), MI - multiplexer interface, MC - micro-computer, CD - colour display (two-dimensional) 4KM - memory with control, D - display, DMA - direct memory access). The numbers indicate the data word length in bit.

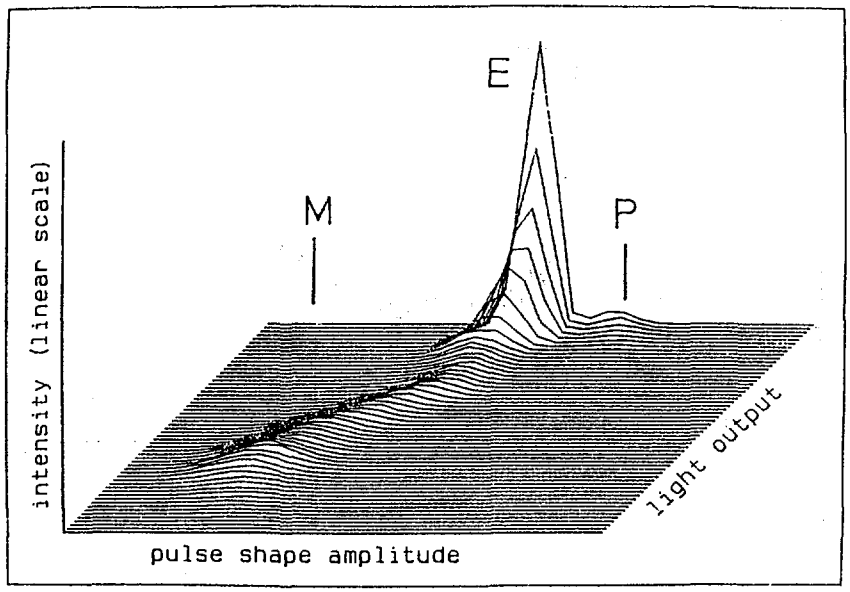

Fig. 3 Two-dimensional particle identification spectrum for neutron detector 1 (light output amplitude, pulse shape amplitude) illustrating the foreground/background relations at high energy (non-correlated spectrum). M - cosmic myon region, E - Compton electron region (γ branch), P - recoil proton region (neutron branch).

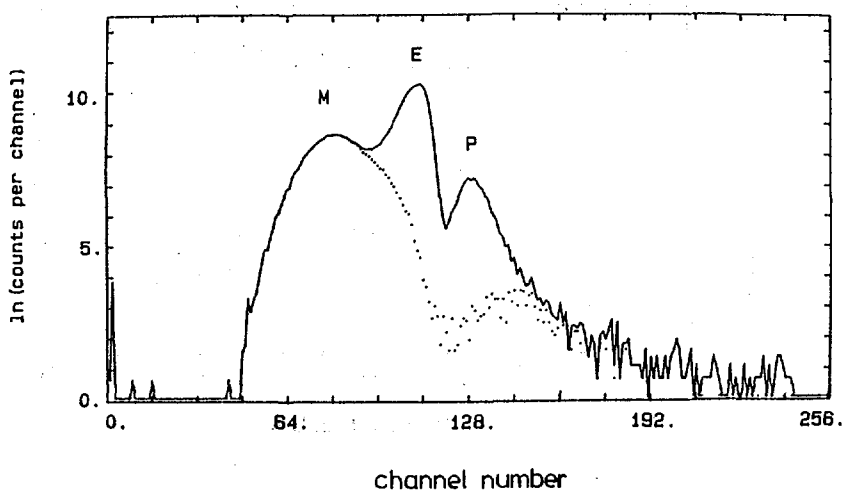

Fig. 4 Pulse-shape amplitude spectrum (logarithmic scale) for two selected LO bias energies (sections of the Fig. 3 spectrum):
2.5 MeV proton energy equivalent (continuous curve),
7.5 MeV proton energy equivalent (dotted curve).

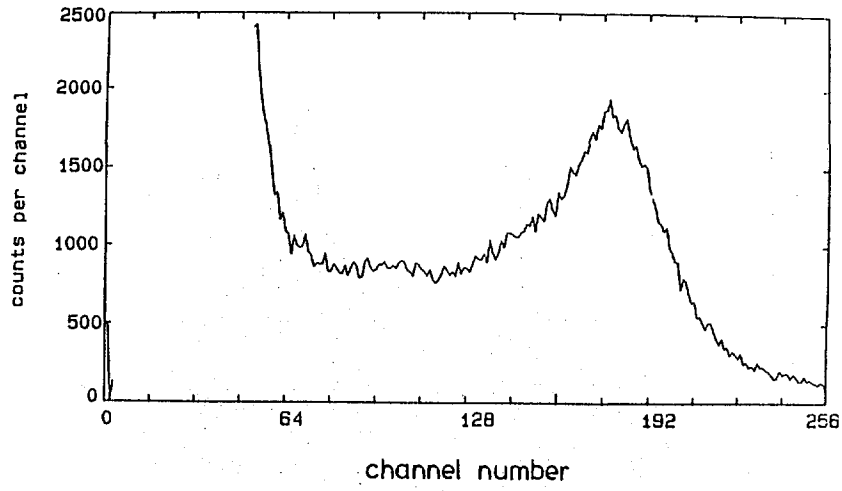

Fig. 5 L0 amplitude spectrum (detector 1) of a 10.5 h run showing the cosmic myon hump at about 11.5 MeV proton energy equivalent (maximum).

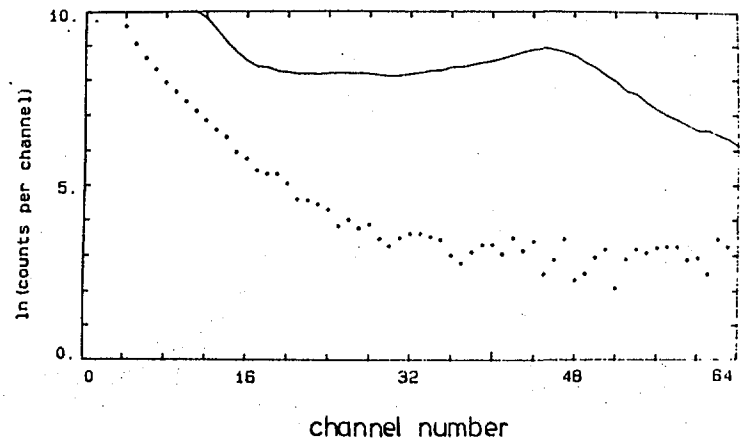

Fig. 6 As Fig. 5, but including the L0 spectrum in coincidence with the neutron identification signal in a logarithmic scale (channels concentrated).

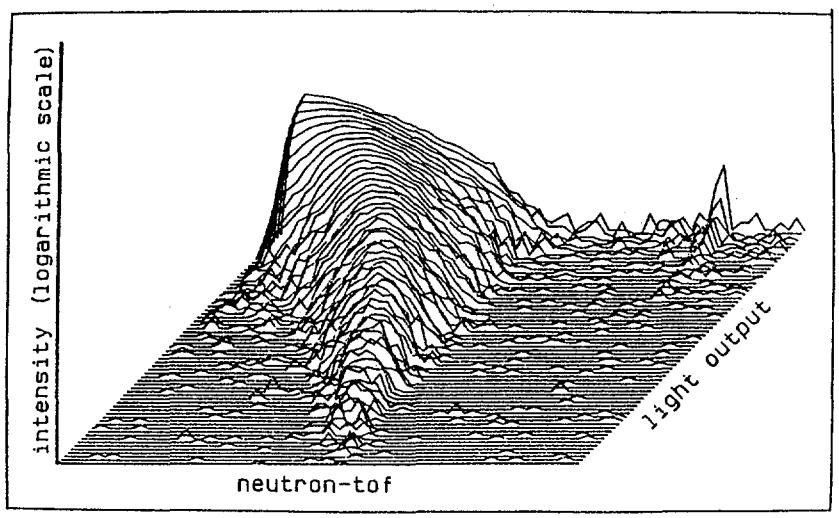

Fig. 7 Two-dimensional neutron spectrum of detector 1 (neutron TOF, LO). The channels of the original spectrum have been concentrated for representation.

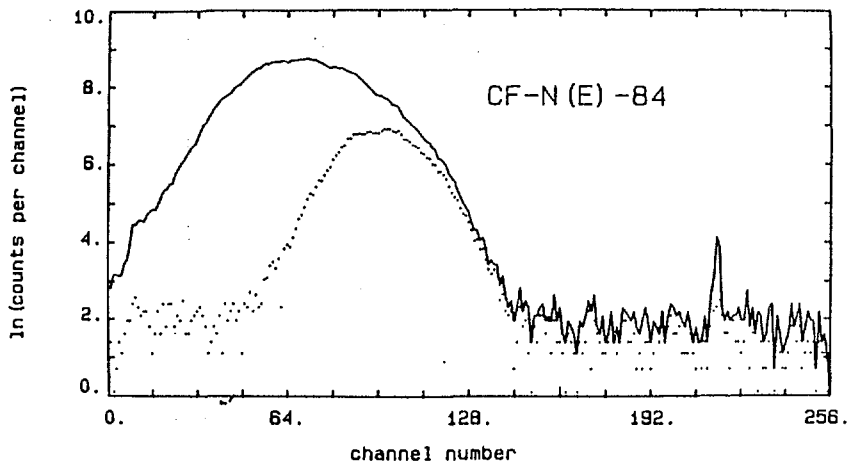

Fig. 8 Typical neutron TOF spectra (logarithmic scale) of detector 1 deduced for two LO bias energies (4.3 and 6.6 MeV proton energy equivalent).

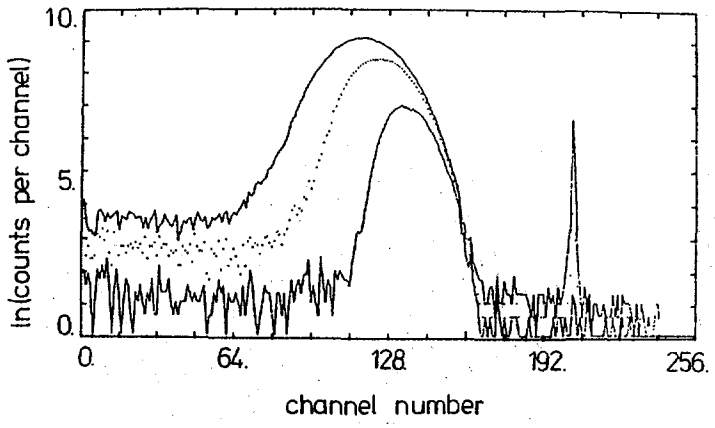

Fig. 9 Typical neutron TOF spectra (logarithmic scale) of detector 2 for three LO bias energies (3.5, 4.5 and 6.5 MeV proton energy equivalent).

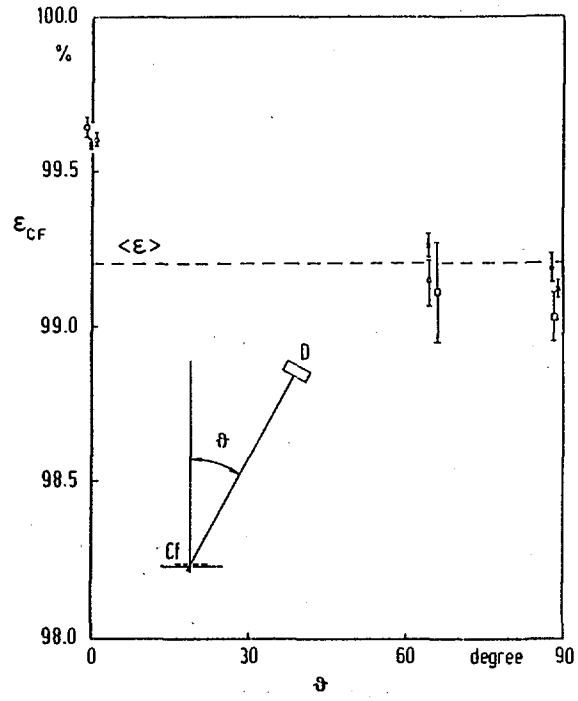

Fig. 10 Fission fragment detection efficiency ε_{cf} in dependence on the position of the neutron detector (angle ϑ). The neutron spectra were analyzed for thresholds of 0.25 (x), 0.5 (o) and 1.0 (□) MeV equivalent electron energy.

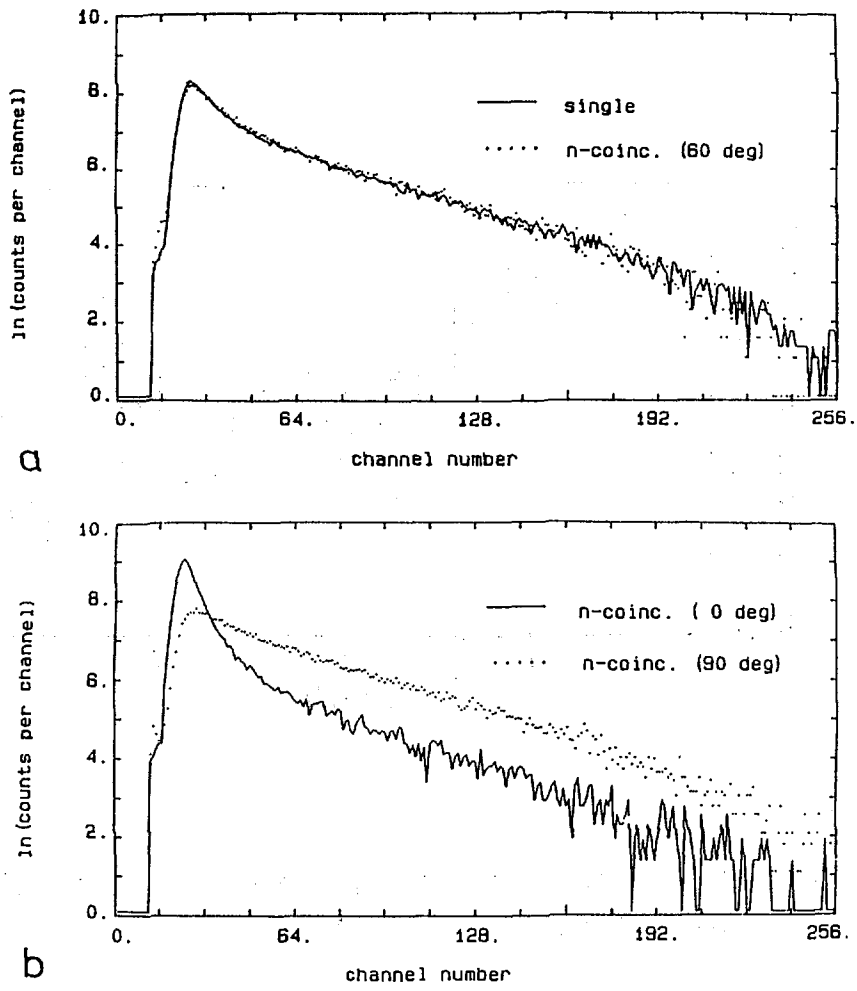

Fig. 11 Fission fragment ΔE-spectra measured without correlation (a, full line) and in coincidence with the neutron detector at 60° (a, dotted), 0° (b, full line), and 90° (b, dotted).

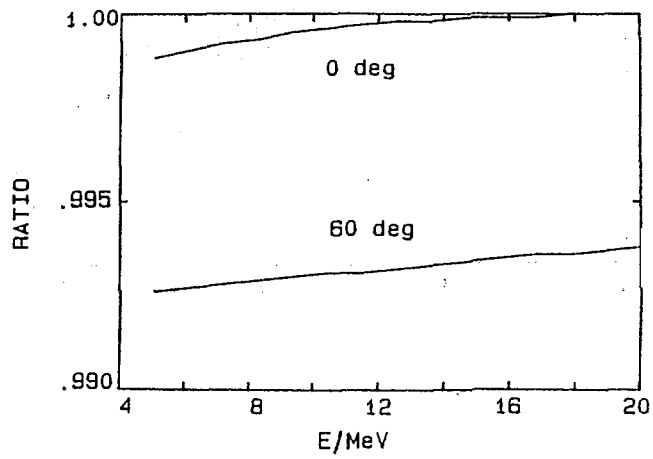

Fig. 12 Ratio of the measurable and the undisturbed Cf neutron spectrum calculated for a 99.2 % fragment detection efficiency.

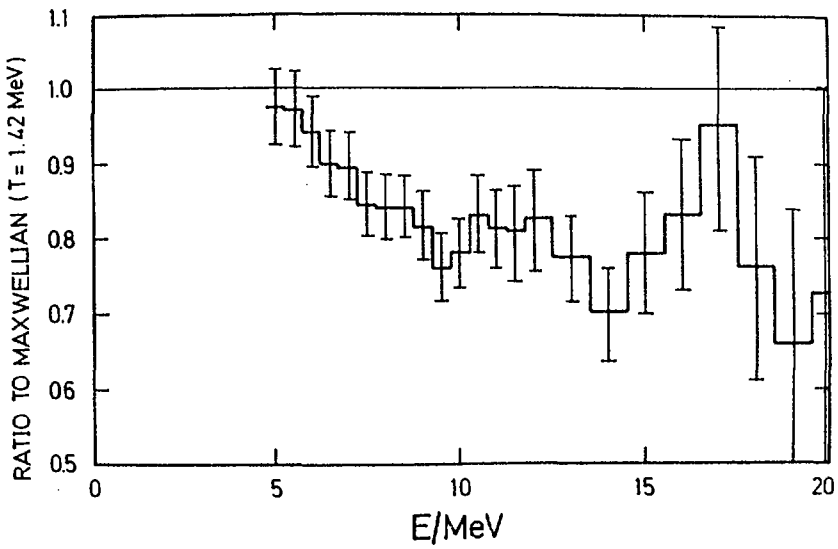

Fig. 13 Final Cf neutron energy spectrum (detector 1) relative to a Maxwellian (T = 1.42 MeV).

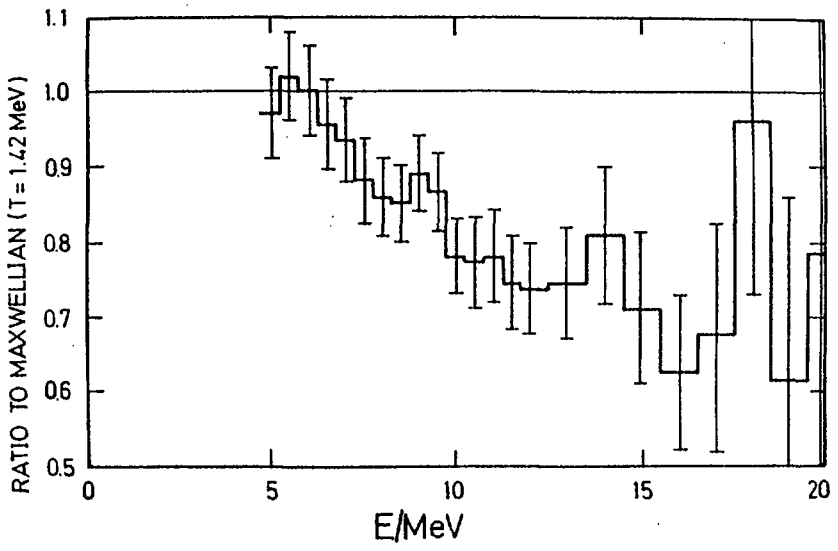

Fig. 14 Final Cf neutron energy spectrum (detector 2) relative to a Maxwellian (T = 1.42 MeV).

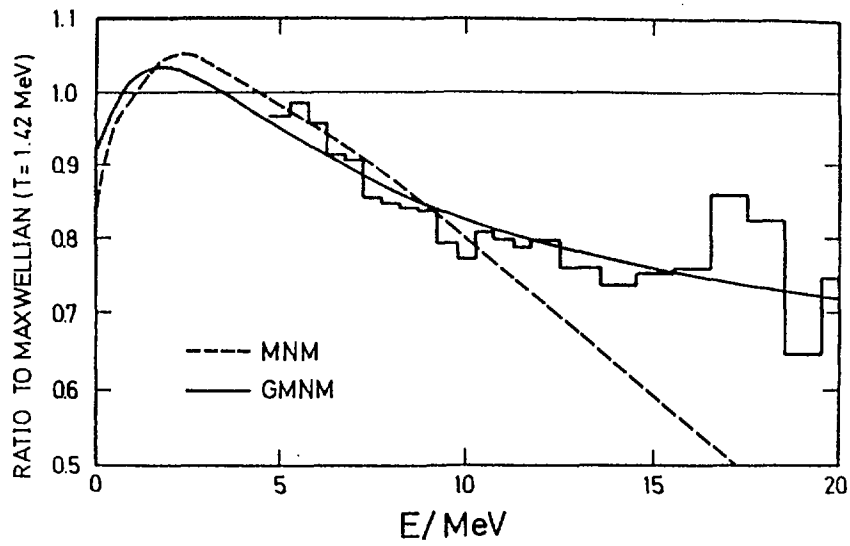

Fig. 15 Final Cf neutron energy spectrum (weighted average of detector 1 and detector 2) in comparison with two statistical-model approaches (MNM - Madland-Nix model[10], GMNM - Generalized Madland-Nix model[11], C = 8.0 MeV calculation).

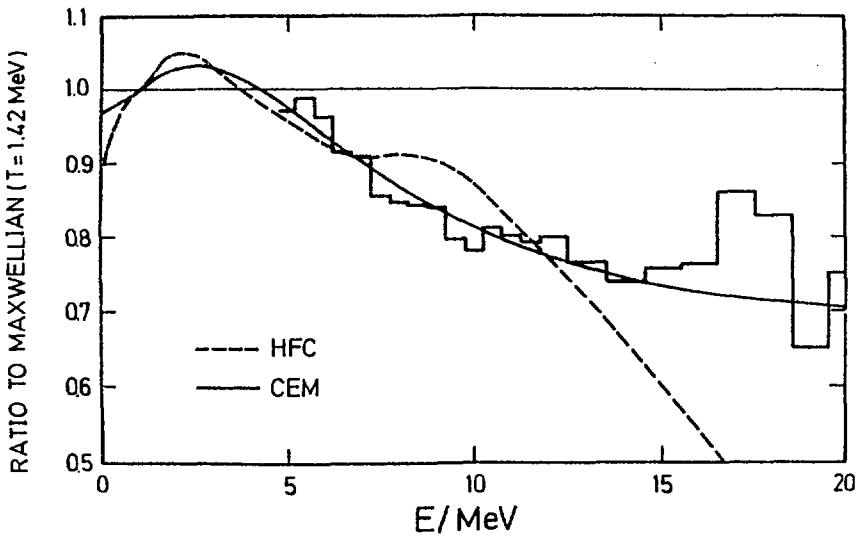

Fig. 16 As Fig. 15, but in comparison with two other theories (CEM - Cascade Evaporation model, HFC - Hauser-Feshbach calculation[13]).

Table 1 Characteristics of the neutron spectrometer

Item	Detector 1	Detector 2
Neutron detector (type, size photomultiplier, timing)	NE213 (12.7 cm x 12.7 cm) XP 2041 constant-fraction trigger	NE213 (12.7 cm x 3.81 cm) XP 2041 constant-fraction trigger
Neutron detector position	0 degrees	60 degrees
flight path	5.905 m	3.275 m
TAC range	250 ns	250 ns
TOF bin width	(1.106 $\pm$ 0.003) ns	(1.068 $\pm$ 0.003) ns
time resolution (FWHM γ peak)	1.5 ns	1.3 ns
γ peak position uncertainty	0.09 ns	0.08 ns
typical uncertainty of LO bias	0.06 MeV	0.06 MeV
total number of fragment signals	$1.5 * 10^{11}$	$8.3 * 10^{10}$

Table 2 Concentrated data of the ^{252}Cf(sf) neutron spectrum. Measurement Cf-N(E)-84TUD/PTB(IAEA) - Detector 1 (0 degrees). E - neutron energy, R - ratio to Maxwellian (T = 1.42 MeV) - average for selected energy bins (bin width: .5 MeV at E < 12 MeV, 1. MeV at E > 12 MeV), N(E) - emission probability (norm 1) - point data, PU - percentage uncertainty (ST - statistical, SY - systematic, TOT - total).

E/MeV	R	N(E)/MeV^{-1}	PU-ST	PU-SY	PU-TOT
5.0	0.9713	.4282E-01	0.3	5.5	5.5
5.5	0.9695	.3152E-01	0.4	5.3	5.3
6.0	0.9397	.2244E-01	0.5	5.2	5.2
6.5	0.8971	.1568E-01	0.6	5.2	5.2
7.0	0.8962	.1143E-01	0.7	5.1	5.1
7.5	0.8447	.7842E-02	0.8	5.1	5.2
8.0	0.8403	.5666E-02	1.0	5.2	5.3
8.5	0.8393	.4102E-02	1.2	5.2	5.3
9.0	0.8165	.2887E-02	1.5	5.3	5.5
9.5	0.7607	.1944E-02	1.7	5.4	5.7
10.0	0.7801	.1438E-02	2.1	5.4	5.8
10.5	0.8298	.1102E-02	2.6	5.5	6.1
11.0	0.8139	.7781E-03	3.1	5.6	6.4
11.5	0.8127	.5586E-03	3.7	5.8	6.9
12.0	0.8278	.4087E-03	4.2	6.0	7.3
13.0	0.7735	.1966E-03	4.1	6.4	7.6
14.0	0.7013	.9145E-04	5.7	6.8	8.9
15.0	0.7783	.5195E-04	7.1	7.3	10.2
16.0	0.8280	.2823E-04	9.2	7.9	12.1
17.0	0.9508	.1652E-04	11.5	8.7	14.4
18.0	0.7619	.6736E-05	17	9.5	20
19.0	0.6599	.2964E-05	25	10.5	27
20.0	0.7305	.1664E-05	35	11.8	37

Table 3 As Table 2, but for detector 2 (60 degrees position)

E/MeV	R	N(E)/MeV^{-1}	PU-ST	PU-SY	PU-TOT
5.0	0.9682	.4268E-01	0.5	5.9	5.9
5.5	1.0248	.3332E-01	0.6	5.8	5.8
6.0	1.0042	.2398E-01	0.6	5.8	5.8
6.5	0.9538	.1667E-01	0.8	5.7	5.8
7.0	0.9337	.1191E-01	0.8	5.6	5.7
7.5	0.8790	.8161E-02	0.9	5.7	5.8
8.0	0.8593	.5794E-02	1.1	5.8	5.9
8.5	0.8534	.4171E-02	1.3	5.9	6.0
9.0	0.8919	.3154E-02	1.7	6.0	6.2
9.5	0.8660	.2213E-02	2.0	6.1	6.4
10.0	0.7811	.1440E-02	2.5	6.2	6.7
10.5	0.7765	.1031E-02	3.0	6.3	7.0
11.0	0.7786	.7444E-03	3.6	6.5	7.4
11.5	0.7463	.5130E-03	4.9	6.8	8.4
12.0	0.7377	.3643E-03	5.4	7.2	9.0
13.0	0.7433	.1889E-03	5.6	7.9	9.7
14.0	0.8090	.1055E-03	7.1	8.3	10.9
15.0	0.7106	.4743E-04	10.0	8.8	13.3
16.0	0.6233	.2125E-04	14.3	9.4	17.1
17.0	0.6783	.1179E-04	18	10.1	21
18.0	0.9590	.8479E-05	21	10.9	24
19.0	0.6140	.2758E-05	37	11.8	39
20.0	0.7853	.1789E-05	53	12.8	55